Inorg. Chem. **2004**, *43*, 4880–4888

Nonexponential Relaxation of the Metastable State of the Spin-Crossover System $[Fe(L)_2](ClO_4)_2 \cdot H_2O$ [L = 2,6-Bis(pyrazol-1-ylmethyl)pyridine]

Cristian Enachescu,[†,‡] Jorge Linares,[†] François Varret,*[,†] Kamel Boukheddaden,[†] Epiphane Codjovi,[†] Sunita Gawali Salunke,[†,§] and Rabindranath Mukherjee[||]

Laboratoire de Magnétisme et d'Optique, CNRS−Université de Versailles, 78035 Versailles, France, Faculty of Physics, University Al. I. Cuza, Bulevard Carol I, 700506 Iasi, Romania, Applied Chemistry Division, Institute of Chemical Technology, University of Bombay, Matunga, Mumbai 400 019, India, and Department of Chemistry, Indian Institute of Technology, Kanpur 208016, India

Received January 14, 2004

The relaxation of the metastable state of the spin-crossover compound $[Fe(L)_2](ClO_4)_2 \cdot H_2O$, with L = 2,6-bis-(pyrazol-1-ylmethyl)pyridine, populated by the LIESST (light induced excited spin state trapping) effect, has been investigated by magnetic measurements. The time dependence of the relaxation curve at several temperatures, starting from different initial states, is in the shape of stretched exponentials, and the thermal variation of the photostationary state under constant photoexcitation is progressive and reversible. These features are satisfactorily modeled by considering noninteracting two-level systems with a distribution of activation energies. A suggested origin for the distribution is the conformational flexibility of the nonplanar heterocyclic ligands. The effect of the intensity distribution during the LIESST process is also accounted for in a simple way.

Introduction

The present study was undertaken in order to accurately investigate the relaxation properties of a pure spin-crossover system with negligible cooperative effects. See for example refs 1 and 2 for recent reviews. Indeed the conversion curve of $[Fe(L)_2](ClO_4)_2 \cdot H_2O$, with L = 2,6-bis(pyrazol-1-ylmethyl)pyridine[3] was reported to be extremely smooth but almost complete. Also the conformational flexibility of the ligand,[3−7] see Figure 1, made the compound a priori interesting. Indeed, the X-ray structure (≈130 K) of the low-spin form of this complex reveals that the two pyrazole mean planes of each ligand make an angle of ∼65 and ∼66° to each other. The pyridine mean plane is tilted to adjacent pyrazole rings within a ligand at angles of ∼47 and ∼62°, ∼39 and ∼66°.[6]

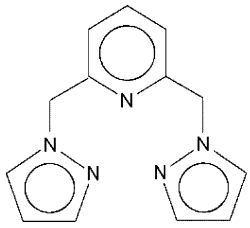

Figure 1. Schematic representation of the tridentate ligand L = 2,6-bis-(pyrazol-1-ylmethyl)pyridine. Free rotations around the N−C and C−C single bonds are responsible for conformational flexibility.

It may be worth recalling that cooperative spin-crossover compounds, e.g. which undergo the abrupt spin transition with thermal hysteresis, also exhibit self-accelerated relaxation of the metastable state,[8] for instance after being

* Author to whom correspondence should be addressed. E-mail: fvarret@physique.uvsq.fr.
[†] Université de Versailles.
[‡] University Al. I. Cuza.
[§] University of Bombay.
[||] Indian Institute of Technology.

(1) Gütlich, P.; Hauser, A.; Spiering, H. *Angew. Chem., Int. Ed. Engl.* **1994**, *33*, 2024.
(2) Varret, F.; Nogues, M.; Goujon, A. In *Magnetism: Molecules to Materials*; Miller J., Drillon, M., Eds.; Wiley-VCH: New York, 2001; Vol. 2, pp 257−295.
(3) Mahapatra, S.; Mukherjee, R. *Polyhedron* **1993**, *12*, 1603.
(4) Mahapatra, S.; Gupta, N.; Mukherjee, R. *J. Chem. Soc., Dalton Trans.* **1991**, 2911.
(5) Mahapatra, S.; Butcher, R. J.; Mukherjee, R. *J. Chem. Soc., Dalton Trans.* **1993**, 3723.
(6) Mahapatra, S.; Butcher, R. J.; Mukherjee, R. *Indian J. Chem.* **2001**, *40A*, 973.
(7) Mukherjee, R. *Coord. Chem. Rev.* **2000**, *203*, 151.
(8) Hauser, A. *Chem. Phys. Lett.* **1992**, *192*, 65.

10.1021/ic049938+ CCC: $27.50
Published on Web 07/09/2004

previously populated by the LIESST (light induced excited spin state trapping[1]) effect. The self-accelerated relaxation is adequately described by a cooperative effect of the steric interactions upon the barrier energy: the relaxation becomes faster and faster while the population of the metastable state becomes smaller and smaller. In most cases, at long times, the relaxation rate slows down and results in the so-called "relaxation tail",[9] which is well-reproduced by models[9,10] accounting for the onset of correlations due to the short-range part of the steric interactions.

We were rather puzzled by the relaxation curves of the present compound, in the shape of stretched exponentials, typical of a *self-decelerated* process. At first, we tried to reproduce them in the frame of the relaxation tail effect, i.e., by a model involving only short-range interactions. But all attempts were unsatisfactory, in addition to the obvious absence of cooperative effects at the thermal transition.

On the other hand, we have considered the possible disorder associated with the effect of the conformational flexibility of the ligand.[3−7] Consequently, following ref 11 for spin-crossover diluted in polymers (see also for polymeric systems refs 12 and 13), we were led to assume a distribution of barrier energies. We have undertaken an extensive experimental study, as a function of temperature, and for different initial populations of the metastable state. We have also followed the thermal evolution of the photostationary equilibrium and finally found useful information from the shape of the photoexcitation curves, i.e., the time dependence of the HS fraction during the LIESST process; see refs 14−16. It was clear that in the absence of cooperativity the quantum yield of the LIESST process[16] should be considered as a constant and that the nonlinear character of the photoexcitation response should be unambiguously attributed to bulk absorption of light in the sample.[8] Therefore the model used here involves both a distribution of barrier energies and a distribution of irradiation intensities.

Experimental Section

Synthesis of the title compound was accomplished following a published procedure.[3,4]

The magnetization curves were recorded using a SQUID magnetometer (Quantum Design MPMS5) operating in the alternative mode, equipped with an optical fiber, made of multiwire silica, for light irradiation in the visible−near-IR range. The flexible end of the optical fiber was connected to a broadband source of light (tungsten halogen lamp, 100 W), through interferential filters (100 nm bandwidth). The optical device around the sample (silica rods) has been described in refs 17 and 18. The sample holder and optical fibers induced a parasitic magnetic contribution which has been recorded separately and systematically subtracted from the data.

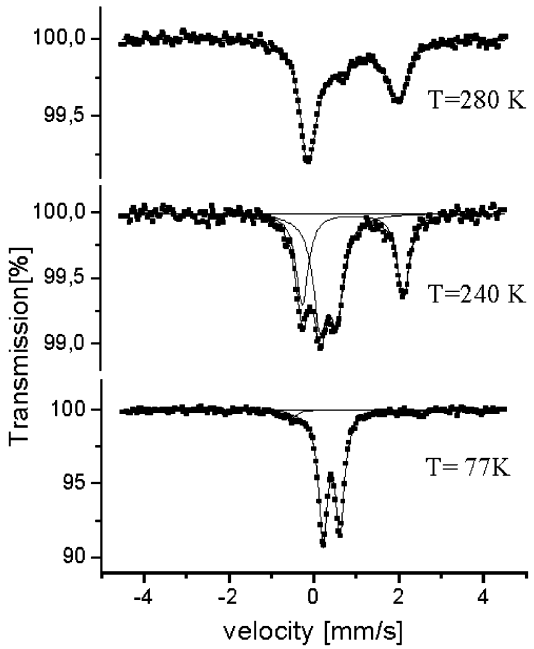

Figure 2. Typical Mössbauer spectra of [Fe(L)$_2$](ClO$_4$)$_2$·H$_2$O, with L = 2,6-bis(pyrazol-1-ylmethyl)pyridine and their least-squares best fits (dynamic model for T = 280 K).

Mössbauer spectra were recorded on a constant-acceleration spectrometer, with a 50 mCi source of ^{57}Co in rhodium matrix. The polycrystalline absorber contained 20 mg of material/cm^2. The typical experimental line width, in the useful velocity range, was ∼0.215 mm·s^{-1}. The spectra, once folded, were fitted without correction for the thickness effect. Least-squares-fitted parameters are given with their standard deviation of statistical origin (in brackets), and isomer shift values refer to metallic iron at room temperature.

Results and Discussion

Equilibrium Properties. Mössbauer spectra have been recorded in order to provide a local probe of the structural quality of the sample and a direct calibration of the magnetic measurements in terms of the high-spin fraction, $n_{HS}(T)$. Typical spectra are shown in Figure 2 and exhibit narrow lines at low temperatures. A small residual HS fraction (∼5%) is detected at the lowest temperature and will be systematically subtracted from the data for the detailed analysis. At higher temperatures, when both HS and LS components are present, sizable line broadening occurs, typical for a dynamic mixture of the spin states[19,20] due to the speeding up of the LS ↔ HS relaxation when both states are populated (Table 1). Using the relaxation model devel-

(9) Romstedt, H.; Hauser, A.; Spiering, H. *J. Phys. Chem. Solids* **1998**, *59*, 265.
(10) Hôo, B.; Boukheddaden, K.; Varret, F. *Eur. Phys. J. B* **2000**, *17*, 449.
(11) Hauser, A.; Adler, J.; Gütlich, P. *Chem. Phys. Lett.* **1988**, *152*, 6.
(12) Richert, R. *Chem. Phys*. **1988**, *122*, 455.
(13) Palmer, R.; Stein, D. L.; Abrahams, E.; Anderson, P. W. *Phys. Rev. Lett*. **1984**, *53*, 958.
(14) Enachescu, C.; Constant-Machado, H.; Codjovi, E.; Linares, J.; Boukheddaden, K.; Varret, F. *J. Phys. Chem. Solids* **2001**, *62*, 1409.
(15) Varret, F.; Boukheddaden, K.; Codjovi, E.; Enachescu, C.; Linarès, J. In *Spin Crossover in Transition Metal Compounds*; Gütlich, P., Goodwin, H., Eds; Topics in Current Chemistry; Springer: Berlin, Germany, in press:
(16) Enachescu, C.; Oetliker, U.; Hauser, A. *J. Phys. Chem*. **2002**, *37*, 9540.
(17) Morscheidt, W.; Codjovi, E.; Jeftic, J.; Linarès, J.; Bousseksou, A.; Constant-Machado, H.; Varret, F. *Meas. Sci. Technol*. **1998**, *9*, 1311.
(18) Codjovi, E.; Morscheidt, W.; Jeftic, J.; Linares, J.; Nogues, M.; Goujon, A.; Roubeau, O.; Constant-Machado, H.; Desaix, A.; Bousseksou, A.; Verdaguer, M.; Varret, F. ICMM'98 (Seignosse, France) Proceedings. *J. Mol. Cryst. Liq. Cryst* **1999**, *335*, 1295.
(19) Adler, P.; Spiering, H.; Gütlich, P. *Hyperfine Interact*. **1988**, *42*, 1035.
(20) Lemercier, G.; Bousseksou, A.; Verelst, M.; Varret, F.; Tuchagues, J. P. *J. Magn. Magn. Mater*. **1995**, *150*, 227.

Table 1. Least-Squares-Fit Parameters of Some Typical Mössbauer Spectra[a]

	assignment LS			assignment HS			A(1):A(2) (%)	
T (K)	IS(1) (mm/s)	QS(1) (mm/s)	$\Gamma(1)^b$ (mm/s)	IS(2) (mm/s)	QS(2) (mm/s)	$\Gamma(2)^b$ (mm/s)	LS:HS	k_{HL} (10^6 s^{-1})
77	0.549(1)	0.397(2)	0.244(2)	1.16(1)	3.01(1)	0.24(4)	95:5(1)	
120	0.538(1)	0.391(1)	0.254(2)	1.12(1)	2.88(1)	0.29(3)	94:6(1)	
160	0.526(1)	0.388(1)	0.246(1)	1.100(4)	2.734(7)	0.25(1)	88:12(1)	
200	0.510(1)	0.388(1)	0.256(2)	1.090(2)	2.258(5)	0.290(7)	73:27(1)	
240	0.480(5)	0.383(6)	0.40(1)	1.055(3)	2.380(7)	0.34(1)	56:44(2)	
$280_{dynamic}$	0.47(1)	*0.383*	0.29(2)	1.014(4)	2.31(1)	0.29(2)	37:63(1)	1.5(1)
$300_{dynamic}$	0.44(1)	*0.383*	*0.28*	1.007(5)	2.16(1)	*0.28*	27:73(1)	1.5(1)

[a] IS and QS respectively are the the isomer shift (referred to metallic iron at room temperature) and the quadrupole splitting. [b] Γ is the Lorentzian line width. The numbers in parentheses are the standard deviations of statistical origin. Italicized values were fixed during the fitting procedure. Due to the lower statistics of the 300 K spectrum, the line width values were constrained, leading to *reduced* statistical standard deviations, with respect to the total uncertainties.

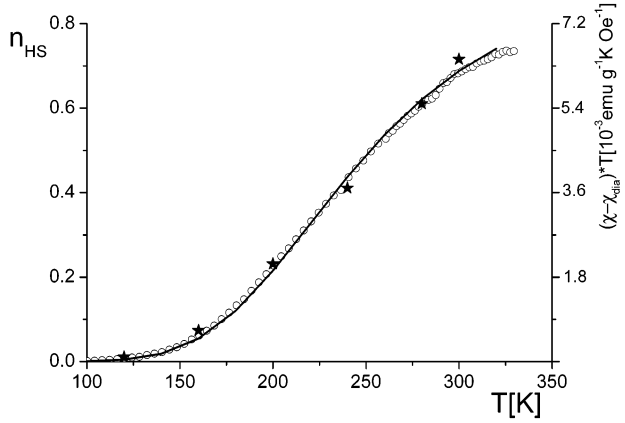

Figure 3. Thermal variation of the high-spin population, from magnetic (○) and Mössbauer (∗) data. $T_{1/2} \sim 250$ K (after removal of the residual HS fraction, 5%). The thermodynamic parameter values for the fit (line) are $\Delta \sim 1250$ K, $g_{HS}/g_{LS} \sim 140$, and $J = 0$.

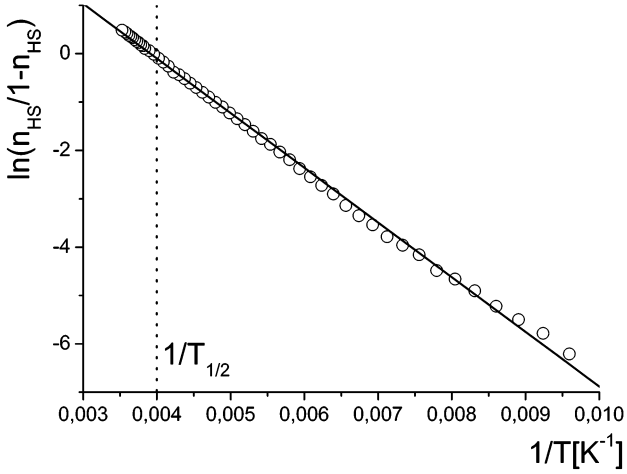

Figure 4. Van't Hoff plot of the spin equilibrium constant, after removal of the residual HS fraction. The linear regression of the curve yields the following thermodynamic parameters: $\Delta H = 9.2$ kJ·mol^{-1}, $\Delta S = 37$ J·K^{-1}·mol^{-1}; i.e., in the two-level description: energy gap, $\Delta = 1130$ K; effective degeneracy ratio, $g_{HS}/g_{LS} = 84$.

oped in refs 19 and 20, the relaxation rate was determined: $k_{HL}(280\text{K}) \sim 1.5 \times 10^6$ s^{-1}. The dynamic fit involves both k_{HL} and k_{HL}, related to n_{HS} and n_{LS} through the detailed balance equation.

Magnetic data were recorded with an ~1 mg sample in the photomagnetic cell of the SQUID magnetometer. After subtraction of the sample holder signal, the magnetic data, plotted in terms of the product χT, are reported in Figure 3, together with the Mössbauer data which provide the calibration of the n_{HS} scale, once corrected for the small residual HS fraction previously quoted. We have also reported the best fit with the usual Ising-like (two-level) model,[21−23] which is well-known to be formally equivalent[24] to the so-called thermodynamic model[25] based on regular solution theory in the Bragg−Williams approach.

The best fit was obtained by neglecting the interaction parameter, and this peculiarity can be better seen from the Van't Hoff plot of the equilibrium constant $K_{equ}(T) = n_{HS}(T)/n_{LS}(T)$; see Figure 4, where the value of the residual HS fraction at low temperature, 5%, was fine-tuned so as to obtain a linear plot down to the lowest temperatures, i.e., the smallest n_{HS} values. The presence of interactions would induce a typical S-shaped deviation centered at the equilibrium temperature,[26] which obviously is not observed here. Due to the different scales of Figures 3 and 4, the least-squares-fitted values of the parameters are not exactly the same. The values obtained in linear scale should be preferred, because the logarithmic scale puts the major emphasis on the low-temperature data, which are obtained with the larger relative errors.

The conversion curve in Figure 3, above the equilibrium temperature, shows a striking similitude to the data of the same system in acetonitrile solution.[27] This is consistent with the conclusion that interactions are negligible in the present compound.

LIESST and Tunneling Relaxation. The compound was photoexcited at 10 K, using green radiation (filter, 550 nm) at different intensities, leading to a progressive increase in the high-spin fraction; see Figure 5. The shapes of the curves $n_{HS}(t)$ obviously depart from simple exponential, and furthermore their asymptotic, i.e., photostationary state, values depend on the light intensity. Deviations from single-exponential shape have been often reported in the literature

(21) Wajnflasz, J. *Phys. Staust Solidi* **1970**, *40*, 537.
(22) Wajnflasz, J.; Pick, R. *J. Phys. Colloq.* **1971**, *32*, C1−91.
(23) Bousseksou, A.; Nasser, J.; Linares, J.; Boukheddaden, K.; Varret, F. *J. Phys. I* **1992**, *2*, 1381.
(24) Zimmermann, R.; König, E. *J. Phys. Chem. Solids* **1977**, *38*, 779.
(25) Slichter, C. P.; Drickamer, H. G. *J. Chem. Phys*. **1972**, *56*, 2142.
(26) Bousseksou, A.; Constant-Machado, H.; Varret, F. *J. Phys. I* **1995**, *5*, 747.
(27) Manikandan, P.; Padmakumar, K.; Justin Thomas, K. R.; Varghese, B.; Onodera, H.; Manoharan, P. T. *Inorg. Chem.* **2001**, *40*, 6930.

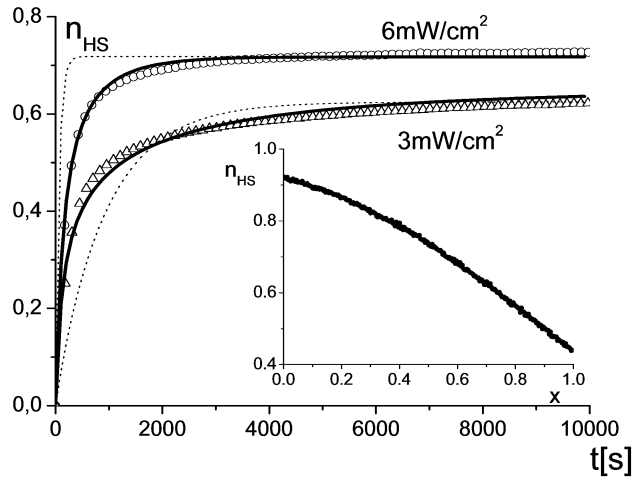

Figure 5. Photoexcitation curve at 10 K, 550 nm, and ~6 and 3 mW·cm^{-2}, from magnetic measurements. Computed curves account for a single distribution of barrier energies (dotted lines) or a joint distribution of barrier energies and light intensities (full lines). Insert: the computed depth profile of the photostationary excited fraction, at 6 mW·cm^{-2}.

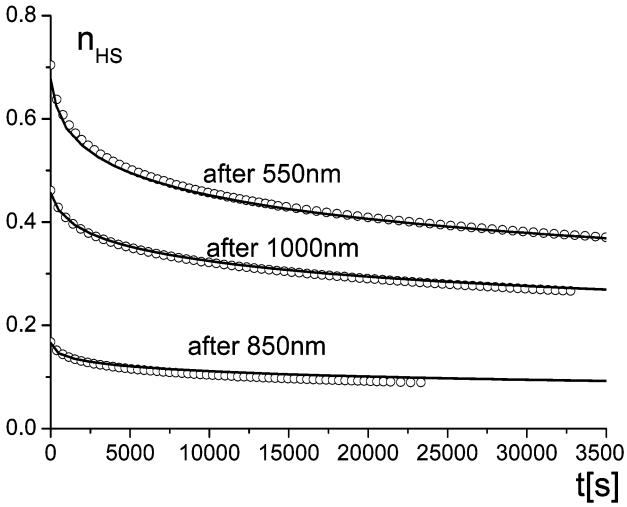

Figure 6. Relaxation curves of the metastable state populated by LIESST, from magnetic measurements at 10 K, starting from photostationary states generated by irradiation with different wavelengths. Best fit computed curves accounting for a single distribution of barrier energies are not shown, since they do not significantly differ from those accounting for the joint distribution of barrier energies and light intensities.

and have been assigned to various origins: bulk absorption of light,[8] including the bleaching effect,[28] competition against cooperative relaxation,[14−16] and nonlinear character of the photoexcitation process.[14−16,29] The dependence of the photostationary state upon the intensity of light observed here makes clear that photoexcitation competes against relaxation, even at low temperature, *i.e. in the tunneling regime.* Due to the absence of interactions, the cooperative relaxation is ruled out. In addition, (i) the eventual nonlinearity of the photoexcitation term should result in an S-shaped distortion of the starting part of the photoexcitation curve, and (ii) the bleaching effect which is often associated with spin-crossover sytems is expected to induce self-acceleration of the photoexcitation rate. Such features are not observed here. Therefore the stretched exponential shape of the photoexcitation curves has to be assigned to the bulk absorption of light in the sample, an effect which will be accounted for in the following. It is also noteworthy that the compound is very dark in the HS state, a property which hinders any efficient bleaching process.

In the course of the study, we had also performed photoexcitations at different wavelengths, to obtain different initial states for the subsequent relaxation experiments.[30] It is clear that such different initial states might have been obtained by using a unique wavelength, with different intensities. In Figure 6 we have reported the relaxation curves measured at 10 K. The central point of the present study is *the stretched exponential shape of these curves.*

The 10 K relaxation data (Figure 6) were first analyzed just assuming a distribution of energy barriers (details of the model are given in the Appendix). In this first approach, the initial state is the photostationary state resulting from the competition between LIESST and relaxation, with the intensity term fitted to the initial n_{HS} value, indeed an average value since the distribution of energy barriers results in a distribution of initial states. Two parameters only are involved in the tunneling regime: $k_{HL}°$ the "central" value of the relaxation rate, and a "modulation factor" accounting for the variation of the barrier energy E_A through a phenomenological parameter, in the form $\exp[\epsilon(E_A^{av} - E_A)]$. In this form, the relative effect associated with the width of the distribution of barrier energies is expressed through the factors $\exp(\pm\epsilon\sigma_E)$, and finally the distribution effect is governed by a single parameter, $\epsilon\sigma_E$. It is worth noting that the above two parameters ($k_{HL}°$, $\epsilon\sigma_E$) are little correlated to each other during the fit of the relaxation curves, since the former governs the time scale and the latter the departure of the curve from the single-exponential shape. Therefore their unambiguous determination was easy. A third parameter was needed for determining the (inhomogeneous) initial state: the intensity term, including absorption cross-section and quantum yield (the latter assumed to be a constant, a good assumption in the absence of cooperativity, according to ref 16).

This way, a satisfactory fit of the relaxation curves could be obtained; see Figure 6. But the set of parameter values, inserted into the master equation (Appendix, eq 3), did not reproduce adequately the photoexcitation curves; see the dotted lines in Figure 5. Obviously the intensity values which fit the photostationary states are too small for reproducing the initial increase of the photoexcitation curves. This is typical for the effect of bulk absorption of light. Consequently we have introduced a distribution of intensities in the sample (see Appendix), following the Beer−Lambert law and neglecting the bleaching effect. The intensity distribution finally is governed by a single additional parameter, the transmission factor of the sample (r). This parameter has generally low values because it takes into account both the

(28) Hauser, A. *Chem. Phys. Lett.* **1986**, *124*, 543,
(29) Ogawa, Y.; Koshihara, S.; Koshino, K.; Ogawa, T.; Urano, C.; Takagi, H. *Phys. Rev. Lett.* **2000**, *84*, 3181.
(30) Enachescu, C.; Linares, J.; Codjovi, E.; Boukheddaden, K.; Varret, F. *J. Optoelectron. Adv. Mater.* **2003**, *5*, 261.

Table 2. Parameter Values Used in the Present Model[a]

experiment	λ (nm)	$I_0\sigma$ (s^{-1})	r	k_{HL}° (s^{-1})	$\epsilon\sigma_E$	$k_{HL}^{\propto}$ (s^{-1})	E_A^{av} K)	σ_E (K)	figure
LIESST 10 K	550	0.005	0.001	5×10^{-5}	5				5
LIESST 10 K	550	0.003	0.001						5
relaxation 10 K	550	*0.005*	0.001						6, 7
relaxation 10 K	850	0.002	0.003						6, 7
relaxation 10 K	1000	0.003	0.005						6, 7
T_{LIESST}	550	*0.005*	*0.001*	*5 × 10−5*	*5*	*2.5 × 10^7*	*800*	425	9
light-induced equilibrium (LIE)	550	*0.005*	*0.001*	*5 × 10−5*	*5*	*2.5 × 10^7*	*800*	400	10, 11
relax. 25 K	550	*0.005*	*0.001*	*5 × 10−5*	*5*	*2.5 × 10^7*	*800*	*400*	12
relax. 40 K	550	*0.005*	*0.001*	*5 × 10−5*	*5*	*2.5 × 10^7*	950	150	12

[a] Italicized values were a priori fixed. All the other ones were fitted to the experimental data. The set of parameters for fitting T_{LIESST} and LIE curves are consistent with the accurate Mössbauer data $k_{HL}(280K) = 1.5 \times 10^6$ s^{-1}.

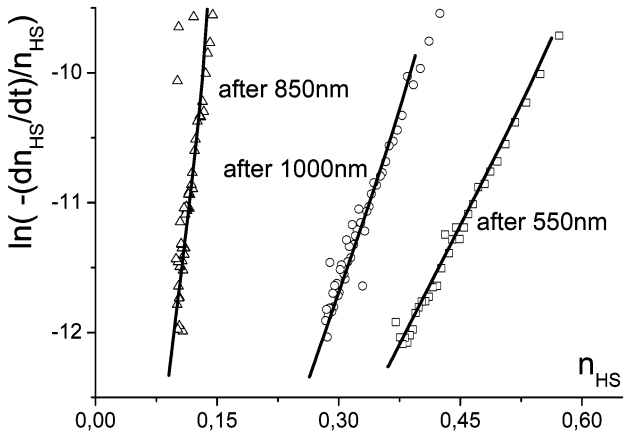

Figure 7. Relaxation at 10 K: experimental data and best fit curve resulting from the joint barrier energy and intensity distribution. Parameter values are listed in Table 2.

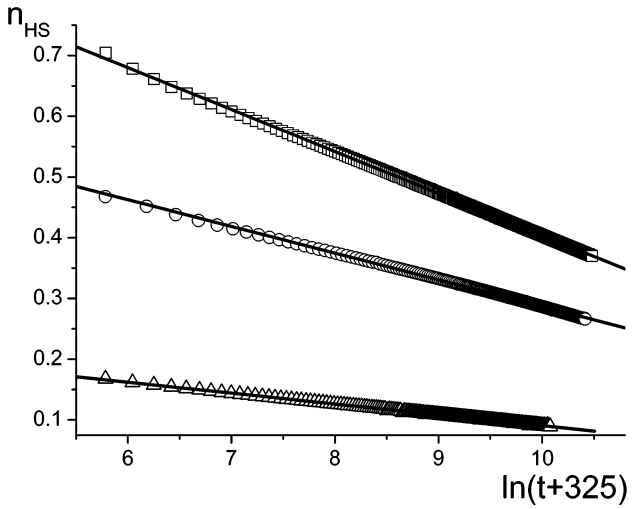

Figure 8. Relaxation at 10 K in the logarithmic time scale: $n_{HS}(t) \sim p \ln(t_0 + t) + Cst$. Fitted values are $t_0 = 325$ s; $p = -0.0691$, -0.0439, -0.0179; and $n_{HS}(t=0) = 1.09$, 0.726, 0.269, from top to bottom, respectively.

absorption and diffusion effects in powder samples. Computations were then performed using a two-dimensional distribution of uncorrelated intensities and barrier energies. The best fitted curves, with the set of parameters listed in Table 2, are drawn in Figures 5 and 6. The agreement with experimental curves is good and therefore emphasizes the crucial effect of bulk absorption upon the data analysis.

We also plotted, in Figure 7, the relaxation data according to the logarithmic scale suitable to the mean-field approach of cooperative effects, i.e., ln k_{HL} vs n_{HS}.[8,31,32] It is known that such a plot results in a straight line as long as the mean-field behavior is obeyed. All literature examples, involving a self-accelerated relaxation due to positive interactions between spin-crossover units, provided a negative slope. In the present case, the slope is positive, and the noticeable point is that the data follow straight lines. We have proceeded to several simulations and have correlated the straight character of the plot to the presence of a wide distribution of barrier energies, such that, at any time during the experiment, there are available relaxation rates. This feature is similar to the magnetic after effect in spin glasses,[33] for which the suited scale is $n(t)$ vs $\ln(t_0 + t)$ time. A plot according to this log−time scale is reported in Figure 8. We noticed that the measured ratio logarithmic slope/initial value $n_{HS}(t=0)$ is roughly the same for the different sets of data recorded at the same temperature; i.e., it seems to be an experimental value irrespective of the initial state. Accordingly, the relaxation data of Figure 7 show straight lines which can be extrapolated to the same $k(n_{HS}=0)$ value. The open question is whether these features are intrinsic to the distributed character of the energy barriers or merely due to the bulk absorption effect, as suggested by specific simulations using the present model. However, a definitive conclusion would require an extensive experimental study as a function of the sample thickness, which is outside the scope of the present study.

Thermal Activation of Relaxation. We have investigated the thermal activation of relaxation by two convenient approaches: (i) the T_{LIESST} procedure, i.e., by heating the photoexcited sample in the dark at a standard heating rate[34] (see Figure 9) and (ii) the thermal variation of the light-induced equilibrium[35] (see Figure 10).

It is worth noting in Figure 9 the low value of the thermal decay temperature of the metastable state, the so-called $T_{LIESST} \sim 38$ K, which is far below the values so far reported for tridentate ligands.[36]

(31) Hauser, A. *J. Chem. Phys.* **1991**, *94*, 2741.
(32) Enachescu, C.; Linares, J.; Varret, F. *J. Phys. Condens. Matter* **2001**, *13*, 2481.
(33) Huang, C. Y. *J. Magn. Magn. Mater*. **1985**, *51*, 1.
(34) Létard, J. F.; Chastanet, G.; Nguyen, O.; Marcen, S.; Marchivie, M.; Guionneau, P.; Chasseau, D.; Gütlich, P. *Monatsh. Chem.* **2003**, *134*, 165.
(35) Boukheddaden, K.; Shteto, I.; Hôo, B.; Varret, F. *Phys. Rev. B* **2000**, *62*, 14806.

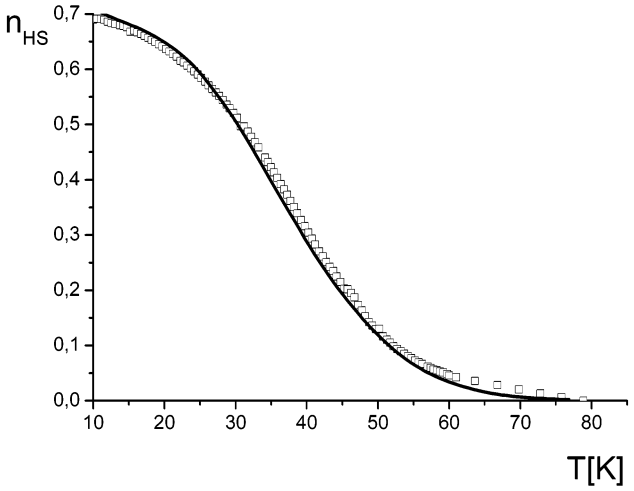

Figure 9. Thermal variation of the high-spin population in the dark, at a heating rate 0.3 K·min^{-1}, after photoexcitation at 550 nm. $T_{LIESST} \sim 38$ K is derived from the inflection point of the experimental curve. Computed curve: $E_A^{av} = 800$ K; $k_{HL}^{\infty} = 2.5 \times 10^7$ s^{-1}; $\sigma_E = 425$ K.

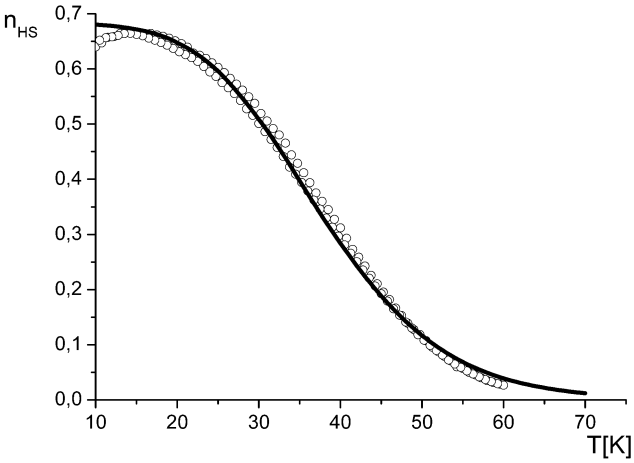

Figure 10. Thermal variation of the spin equilibrium under permanent irradiation at 550 nm, ~6 mW·cm^{-2}, and 0.04 K·min^{-1}, from magnetic measurements. The low-temperature variation of the magnetic signal may be attributed to zero-field-splitting effect of HS Fe^{II}. The narrow loop is purely kinetic. Computed curve: $E_A^{av} = 800$ K; $k_{HL}^{\infty} \sim 2.5 \times 10^7$ s^{-1}; $\sigma_E = 400$ K.

Figure 10 illustrates the competition between photoexcitation and relaxation, which results in a *reversible* temperature-dependent equilibrium between the spin states, the so-called photostationary state. The absence of light-induced instability,[37,38] i.e., the absence of light-induced thermal hysteresis loop (LITH) as termed by Olivier Kahn and collaborators,[39] is consistent with the lack of cooperativity already reported. The small difference between the warming and heating branches can be entirely attributed to the kinetic aspect of the experiment, in other words to the finite value of the temperature sweeping rate.

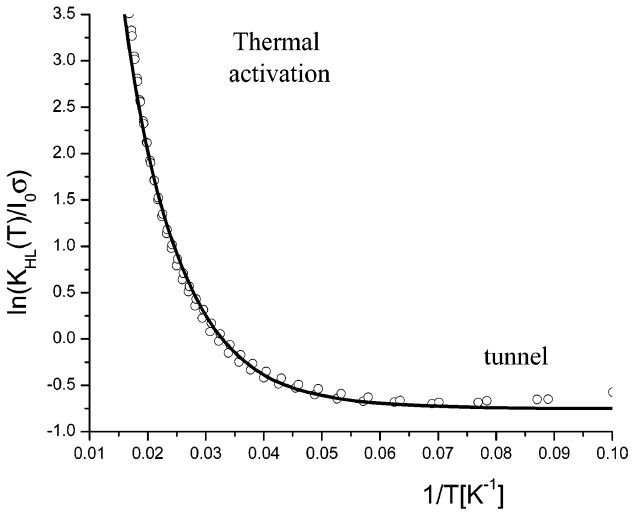

Figure 11. Thermal variation of the spin equilibrium under permanent irradiation, in Arrhenius plot. Computed curve: $E_A^{av} = 800$ K; $k_{HL}^{\infty} \sim 2.5 \times 10^7$ s^{-1}; $\sigma_E = 400$ K.

The light-induced equilibrium data at constant intensity of irradiation, given in Figure 10, were easily transformed into relaxation rate data, as follows. Assuming the spontaneous k_{LH} rate to be negligible at low temperatures, the master equation (Appendix, eq 3) at equilibrium ($dn_{HS}/dt = 0$) yields: $K_{equ} = n_{HS}/n_{LS} = I_0\sigma/k_{HL}$ = excitation rate/relaxation rate. In other words the inverse equilibrium constant measures the relaxation rate in photoexcitation rate units. Using the experimental value $I_0\sigma = 0.005$ s^{-1}, we have derived the relaxation rate data, which we have plotted in logarithmic scale as a function of the inverse temperature; see Figure 11. Such an Arrhenius plot of the relaxation rate provides an independent determination of the average barrier energy and the frequency factor. Accounting for the high-temperature data, including those from the dynamic Mössbauer spectra, the following values were derived: $E_A^{av} \sim 800$ K; $k_{HL}^{\infty} \sim 2.5 \times 10^7$ s^{-1}. A crucial point was the value of the frequency factor, which is consistent with the admitted range of values for the Fe^{II} spin conversion.[40]

Relaxation curves have also been recorded, in the dark, at several temperatures; see Figure 12. Again the stretched exponential character was observed. A difficulty inherent in such experiments is the waiting time which is needed for warming up the sample from the photoexcitation temperature to the experimental temperature. During the waiting time, the system decays in an uncontrolled way, and, obviously, the faster the relaxation, the more important the waiting time effect.

Quantitative Analysis of the Thermally Activated Relaxation. We have analyzed the whole set of data, using the tractable approximation which consists of adding up the tunneling and thermal activation terms: [34]

$$k_{HL}(T) = k_{HL}^{\circ} + k_{HL}^{\infty} \exp(-E_A/k_BT) \qquad (1)$$

(36) Marcen, S.; Lecren, L.; Capes, L.; Goodwin, H. A.; Létard, J. F. *Chem. Phys. Lett.* **2002**, *358*, 87.
(37) Desaix, A.; Roubeau, O.; Jeftic, J.; Haasnoot, J. G.; Boukheddaden, K.; Codjovi, E.; Linares, J.; Nogues, M.; Varret, F. *Eur. Phys. J. B* **1998**, *6*, 183.
(38) Varret, F.; Boukheddaden, K.; Jeftic, J.; Roubeau, O. ICMM'98 (Seignosse, France), Proceedings. *J. Mol. Cryst. Liq. Cryst* **1999**, *335*, 1273.
(39) Letard, J. F.; Guionneau, P.; Rabardel, L.; Howard, J. A. K.; Goeta, A. E.; Chasseau, D.; Kahn, O. *Inorg. Chem.* **1998**, *37*, 4432.
(40) Hauser, A. *Coord. Chem. Rev.* **1991**, *111*, 275.

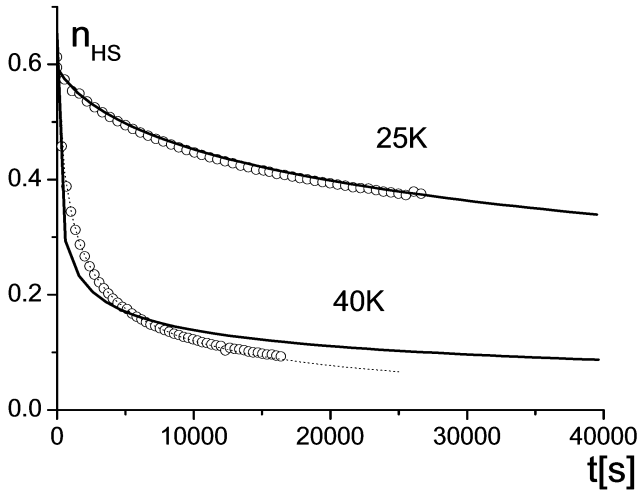

Figure 12. Relaxation curves at several temperatures from magnetic data. Computed curves with high-temperature data (full lines): $E_A^{av} = 800$ K; $k_{HL}^{\infty} \sim 2.5 \times 10^7$ s^{-1}; $\sigma_E = 400$ K. The dotted line results from best-fitted parameters at 40 K: $E_A^{av} = 950$ K; $k_{HL}^{\infty} \sim 2.5 \times 10^7$ s^{-1}; $\sigma_E = 150$ K.

where k_{HL}° is the tunneling rate, E_A the barrier energy, and k_{HL}^{∞} the frequency factor of the thermally activated regime. The tunneling rate value has been determined in the previous section, with the central value $k_{HL}^{\circ} \sim 5 \times 10^{-5}$ s^{-1} and the modulation factor $\epsilon\sigma_E \sim 5$.

We first analyzed the T_{LIESST} (Figure 9) and light-induced equilibrium (Figure 10) data, accounting for uncorrelated distributions of activation energies and irradiation intensities. A satisfactory curve was immediately obtained by taking the previously determined (average) activation energy and frequency factor and only fitting the distribution width $\sigma_E \sim 425$ or 400 K for Figures 9 or 10, respectively.

The agreement was less satisfactory with the relaxation curve at 40 K (see Figure 12) using the whole set of parameters so far derived. A possible reason for this discrepancy is the large waiting time (~7 min). Obviously, the determination of relaxation rates was by no means possible on only the basis of isothermal relaxation curves in the dark. We stress that the thermal decay curve in the dark and the light-induced equilibrium thermal variation offer the priceless advantage that the state of the system remains well-controlled at any time.

Another origin for the possible discrepancies may lie in the approximations made for the photoexcitation model. Also, the thermal effect may sizably warm the sample during photoexcitation, and consequently affect the data, through the derivation $\chi T \rightarrow n_{HS}$. However, the consistence of the data provided by the thermal decay curve in the dark and the light-induced equilibrium suggests that such a thermal effect did not sizably disturb the investigation of the thermally activated regime.

Discussion and Conclusion

The major point to be discussed is the origin of the distribution of relaxation rates. It can be understood as a consequence of a structural disorder associated with the flexibility of the ligand. The Fe(II) complex considered here is indeed special because the ligand is conformationally flexible. The following observations support our hypothesis.

(i) In the X-ray structures of six-coordinate complexes such as $[Fe(L)_2](ClO_4)_2$,[6] $[Fe(L')_2](ClO_4)_2 \cdot MeCN$,[27] $[Fe(L')_2](PF_6)_2$,[27] $[Fe(L')_2](BPh_4)_2 \cdot 2MeCN$,[27] $[Fe(L'')_2](ClO_4)_2$,[5] and also of *fac*-$[ReI(CO)_3(L')]$ [41] [L′ = 2,6-(3,5-dimethylpyrazol-1-ylmethyl)pyridine and L″ = 2-(pyrazol-1-ylmethyl)-6-(3,5-dimethylpyrazol-1-ylmethyl)pyridine; L′ and L″ are closely similar to L, with both the pyrazole rings in L substituted by methyl groups at the 3,5-positions (L′) and with one pyrazole ring in L substituted by methyl groups at the 3,5-positions and the other pyrazole ring in L substituted by methyl groups at the 3,5-positions (L″)], the ligands are in boat conformations. Moreover, it should be noted here that the ligands adopt a *mer* conformation about the metal atom. This is true for all reported structures of the ligands L/L′/L″.[7]

(ii) The average Fe−N(pyridine) bond lengths in $[Fe(L'')_2](ClO_4)_2$ at 173 K are much longer than those in $[Fe(L')_2](ClO_4)_2 \cdot MeCN$, $[Fe(L')_2](BPh_4)_2 \cdot 2MeCN$, and $[Fe(L')_2](PF_6)_2$, at room temperature.[5,27] Such differences in metric parameters observed for closely similar compounds were rationalized due to fluxional behavior of ligand.[27]

(iii) It was reported that the structurally characterized compounds $[Fe(L')_2](ClO_4)_2 \cdot MeCN$ and $[Fe(L')_2](PF_6)_2$ undergo a temperature-dependent conversion between two forms, possibly from a *mer* to *fac* isomer or a boat to chair conformation.[27] Thermally driven interconversion of high-spin and low-spin forms of $[Fe(L')_2](ClO_4)_2 \cdot MeCN$ was considered to be promoted by the *mer* ↔ *fac* change in conformation. They reasoned further that the chelate ring undergoes a change from boat at room temperature to chair at low temperature, creating two different structural forms.[27] Such a situation was observed before.[7,42]

(iv) Interestingly, the dynamics involving the molecular rearrangement of ligand L′ in structurally characterized Cu(I) complexes have been demonstrated by Manikandan et al.[43]

(v) As only one form of the ligand (*mer* conformation) was observed in the X-ray structures of $[Fe(L)_2](ClO_4)_2 \cdot H_2O$,[6] $[Fe(L')_2](ClO_4)_2 \cdot MeCN$,[27] $[Fe(L')_2](PF_6)_2$,[27] $[Fe(L')_2](BPh_4)_2 \cdot 2MeCN$,[27] and $[Fe(L'')_2](ClO_4)_2$,[5] it could be argued that what one sees as *mer* conformation of a ligand is essentially the time-averaged structure of the two conformers *fac* and *mer*,[27] with predominance of *mer* conformation due to steric reason.

(vi) At 233 K in their variable-temperature ^{1}H NMR study on $[Fe(L')_2](ClO_4)_2 \cdot MeCN$ the peaks were more spread out compared to the situation at 333 K.[27] The authors argued that such an observation not only supports the thermally driven interconversion of low-spin and high-spin forms but also supports increased population of the low-spin form at higher temperatures, due to "fluxional" behavior of the ligand conformation.[27]

(41) Orrell, K. G.; Osborne, A. G.; da Silva, M. W.; Hursthouse, M. B.; Coles, S. J. *Polyhedron* **1997**, *16*, 3003.
(42) House, D. A.; Steel, P. J.; Watson, A. A. *Aust. J. Chem.* **1986**, *39*, 1525.
(43) Manikandan, P.; Moni, M. S.; Varghese, B.; Manoharan, P. T. *J. Chem. Soc., Dalton Trans.* **1998**, 3219.

The above findings clearly reinforce our argument that ligand L is conformationally flexible, and the following generalization emerges. For ligand L, there is the possibility of a *fac* ↔ *mer* change in ligand conformation or change in chelate ring boat ↔ chair conformation, when bound to a metal ion.[27]

Final proof of our hypothesis came from our recent results. Very recently we have synthesized a new compound [(L)-Co(H$_2$O)$_3$]Cl$_2$ and structurally characterized it at 100 K. We note that in this compound the ligand adopts facial coordination to the metal ion. To the best of our knowledge, this is the first time that a complex of L has been synthesized and structurally characterized revealing that it coordinates in facial form.[44]

A second point is the low value of the thermal decay temperature, $T_{LIESST} \sim 38$ K. We follow the analysis proposed by Létard et al.,[36] based on a large compilation of experimental values, which states that the experimental T_{LIESST} and $T_{1/2}$ data can be correlated within a given series of compounds. The phenomenological law, consistent with the inverse gap law,[40] is expressed: $T_{LIESST} \sim T_0 - 0.3T_{1/2}$, where T_0 mainly depends on the denticity of the ligand. The T_0 value derived here, 113 K, compares to the values reported for the monodentate and bidentate cases (110, 120 K) and lies far below the value assigned to other tridentates ligands (150 K). We interpret this result as a consequence of the flexibility of the ligand, which drastically reduces the stiffness of the transition metal surroundings, with respect to rigid tridentate ligands. We accordingly suspect that the conformational lability of the ligand might result in low-symmetry distortion modes with low barrier energies, which make the complete description of the thermally activated tunneling regime a very difficult task. Very recently a similar example of T_{LIESST} unexpectedly low for a complex of the tridentate ligand TRIM was presented at a CNRS meeting.[45] TRIM is a tridentate ligand[46] possessing single bonds between organic rings, also allowing conformational flexibility.

We are looking for similar relaxation properties in further compounds also containing flexible ligands. The flexibility of the ligand is also expected to induce specific responses to external stimuli such as hydrostatic pressure.

Acknowledgment. We are indebted to CNRS for financial support, to the Indo-French seminar (Bangalore 2000) for providing an excellent meeting opportunity, to the French government for postdoctoral grant (S.G.S.), and to the NATO for Collaborative Linkage Grant PST.CGL.978097 between Versailles and Iasi Universities. R.M. gratefully acknowledges financial support from the Department of Science and Technology, Government of India. We also thank Dr Azzedine Bousseksou for helpful discussions and for providing the computer program of dynamic Mössbauer spectra developed in ref 19, Prof. J.-C. Micheau for a helpful discussion on the properties of photochromic organic systems, and Dr. Habil. J.-F. Létard and Prof. A. Hauser for friendly discussions about T_{LIESST} and relaxation models.

Appendix

The relaxation rate is written in the following[30] as the sum of a tunneling term and a thermal activation regime term:

$$k_{HL}(T) = k_{HL}^{\circ} + k_{HL}^{\infty}\exp(-E_A/k_BT) \quad (1)$$

where k_{HL}° is the tunneling rate, E_A the barrier energy, and k_{HL}^{∞} the frequency factor of the thermally activated regime (approximate metal−ligand stretching vibrations $\sim 10^{13}$ s^{-1}).

As a consequence of the conformational disorder, the tunneling and thermal activation terms are distributed. For simplicity, we have introduced a Gaussian distribution of activation energies (average value E_A^{av}, standard deviation σ_E) and considered a phenomenological correlation between the tunneling rates and activation energies. The system is considered to be made up of independent spin-crossover units, having E_A with probability $p(E_A) \sim \exp[-(E_A^{av} - E_A)^2/2\sigma_E^2]$, and a relaxation rate expressed as follows:

$$k_{HL}(T,E_A) = k_{HL}^{\circ}\exp[\epsilon(E_A^{av} - E_A)] + k_{HL}^{\infty}\exp(-E_A/k_BT) \quad (2)$$

where k_{HL}° is the reference tunneling rate and ϵ the phenomenological factor correlating activation energies and tunneling rates. The ϵ-value, to be determined from the experiments, should hopefully provide some information on the origin of the distribution (Huang−Rhys factor, energy gap, and vibration frequency).

When photoexcitation and relaxation processes are both present, the evolution of the system obeys the so-called master equation. A simple expression follows, considering a constant quantum yield, and neglecting the LS → HS process (which requires the temperature to be far from $T_{1/2}$):

$$dn_{HS}/dt = I\sigma(1 - n_{HS}) - n_{HS}k_{HL}(T) \quad (3)$$

where $I\sigma$ is the transition rate for a molecular unit to switch LS → HS, with I the beam intensity and σ the absorption cross-section of the sample.

The effect of the bulk absorption of light introduces an intensity distribution, uncorrelated to the barrier energy distribution. Assuming a homogeneous sample, made of successive planar layers at depth x, the measured signal is written as follows:

$$\bar{n}(t) = (1/X)\int_0^X n(t,x)\,dx \quad (4)$$

where the intensity of the light exclusively depends on the depth x, according to the Beer−Lambert law:

Following ref 13, it is convenient integrating over the-variable I. After straightforward transformation the integral the relationship is written as follows:

$$I(x) = I_0\exp(-\alpha x) \quad (5)$$

(44) Balamurugan, V.; Mukherjee, R. Unpublished results.
(45) Bousseksou, A.; Bruefel, N. Private communication at CNRS GDR2429 meeeting (Collonges-la-Rouge, France, October 2003).
(46) Mulliez E., *Tetrahedron Lett.* **1989**, *30*, 6169.

$$\bar{n}(t) = (1/(\ln r))\int_{rI_0}^{I_0}(n(t,I)/I)\,\mathrm{d}I \qquad (6)$$

with $r = \exp(-\alpha X)$. Actually, the intensity is distributed according to the normalized probability law $P(I) = 1/(I \ln r)$. Finally, the bulk absorption effect in the present approximation (no bleaching) involves a single parameter, which is the transmission coefficient of the sample for the considered wavelength. For simplicity, the spectral width of the irradiation light was neglected. It was expected to modulate the depth profile of the photoexcited fraction, and the possible effect of such a modulation was discarded in the present phenomenological approach.

IC049938+